Eden Yifrach[a], Markus Rudowitz[a], Luis Daniel Cruz-Zaragoza, Asa Tirosh, Zohar Gazi, Yoav Peleg, Markus Kunze, Miriam Eisenstein, Wolfgang Schliebs*, Maya Schuldiner*, Ralf Erdmann* and Einat Zalckvar*

Determining the targeting specificity of the selective peroxisomal targeting factor Pex9

https://doi.org/10.1515/hsz-2022-0116
Received February 6, 2022; accepted August 24, 2022; published online October 24, 2022

Abstract: Accurate and regulated protein targeting is crucial for cellular function and proteostasis. In the yeast *Saccharomyces cerevisiae*, peroxisomal matrix proteins, which harboring a Peroxisomal Targeting Signal 1 (PTS1), can utilize two paralog targeting factors, Pex5 and Pex9, to target correctly. While both proteins are similar and recognize PTS1 signals, Pex9 targets only a subset of Pex5 cargo proteins. However, what defines this substrate selectivity remains uncovered. Here, we used unbiased screens alongside directed experiments to identify the properties underlying Pex9 targeting specificity. We find that the specificity of Pex9 is largely determined by the hydrophobic nature of the amino acid preceding the PTS1 tripeptide of its cargos. This is explained by structural modeling of the PTS1-binding cavities of the two factors showing differences in their surface hydrophobicity. Our work outlines the mechanism by which targeting specificity is achieved, enabling dynamic rewiring of the peroxisomal proteome in changing metabolic needs.

Keywords: peroxisome; Pex5; Pex9; protein targeting; PTS1; *Saccharomyces cerevisiae*.

Introduction

Targeting proteins to their correct cellular location is a fundamental process for the life of every organism. In eukaryotes, nearly all proteins are synthesized by ribosomes in the cytosol and a large fraction of these must be targeted to their designated compartment to function properly (Hegde and Zavodszky 2019). Targeting to the appropriate compartment allows a protein to form the necessary interactions with its partners and participate in biological networks such as signaling and metabolic pathways (Laurila and Vihinen 2009). The efficacy and accuracy of the targeting machinery also prevent the protein from mislocalizing to other organelles or aggregating in the cytosol. For these reasons, mutations affecting the targeting of individual proteins or the targeting machinery itself can have severe functional consequences on cells and cause disease (Schaeffer, Creatore and Rampoldi 2014).

While organelles have distinct molecular machineries for directed targeting, they often share fundamental features such as the reliance on a targeting signal within the nascent protein and its recognition by a destination-specific targeting factor. Thus, the fidelity of cellular spatial organization relies critically on the specificity by which signals on the targeted proteins are recognized by their associated targeting factors (Aviram and Schuldiner 2017; Hegde and Zavodszky 2019).

Peroxisomes are organelles with complex and fascinating targeting machinery. Peroxisomes perform and regulate a myriad of metabolic activities, such as degradation of fatty acids and regulation of redox homeostasis (Islinger et al. 2018). For these processes to occur, proper import of lumenal enzymes is essential. Most peroxisomal matrix (lumen) proteins are targeted by recognition of either one of two

[a]Eden Yifrach and Markus Rudowitz contributed equally to this work.

***Corresponding authors: Wolfgang Schliebs and Ralf Erdmann**, Department of Systems Biochemistry, Institute of Biochemistry and Pathobiochemistry, Ruhr-University Bochum, Bochum, Germany, E-mail: wolfgang.schliebs@ruhr-uni-bochum.de (W. Schliebs), ralf.erdmann@ruhr-uni-bochum.de (R. Erdmann). https://orcid.org/0000-0003-2762-3403 (W. Schliebs). https://orcid.org/0000-0001-8380-0342 (R. Erdmann); **Maya Schuldiner and Einat Zalckvar**, Department of Molecular Genetics, The Weizmann Institute of Science, Rehovot 7610001, Israel, E-mail: maya.schuldiner@weizmann.ac.il (M. Schuldiner), einat.zalckvar@weizmann.ac.il (E. Zalckvar). https://orcid.org/0000-0001-9947-115X (M. Schuldiner). https://orcid.org/0000-0003-3724-3965 (E. Zalckvar)
Eden Yifrach, Zohar Gazi and Miriam Eisenstein, Department of Molecular Genetics, The Weizmann Institute of Science, Rehovot 7610001, Israel. https://orcid.org/0000-0001-5074-0048 (E. Yifrach)
Markus Rudowitz and Luis Daniel Cruz-Zaragoza, Department of Systems Biochemistry, Institute of Biochemistry and Pathobiochemistry, Ruhr-University Bochum, Bochum, Germany. https://orcid.org/0000-0001-9568-0245 (L.D. Cruz-Zaragoza)
Asa Tirosh and Yoav Peleg, Life Sciences Core Facilities (LSCF), The Weizmann Institute of Science, Rehovot 7610001, Israel
Markus Kunze, Department of Pathobiology of the Nervous System, Center for Brain research, Medical University of Vienna, Spitalgasse 4, A-1090 Vienna, Austria

constitutive targeting factors, Peroxin 5 (Pex5) and Peroxin 7 (Pex7). Pex5 and Pex7 recognize proteins with a Peroxisomal Targeting Signal (PTS) type I or type II, respectively, and shuttle them to the organelle (Walter and Erdmann 2019). The PTS1 is defined as a tripeptide at the C terminus (C′) of the protein with additional amino acids upstream also contributing to the binding (DeLoache, Russ and Dueber 2016; Fodor et al. 2012; Hagen et al. 2015; Hochreiter et al. 2020; Lametschwandtner et al. 1998; Stanley et al. 2006). The canonical yeast PTS1 tripeptide contains a small uncharged residue (serine (S)/alanine (A)), followed by a positively charged residue (arginine (R)/lysine (K)/histidine (H)), and at the extreme C′ a leucine (L) or phenylalanine (F) (Brocard and Hartig 2006). Some additional residues extend the canonical sequence in yeast, however, they are currently found only in a handful of proteins (Yifrach et al. 2021).

We previously identified an additional targeting factor, Peroxin 9 (Pex9), which is expressed in yeast under specific metabolic conditions, such as the fatty acid oleate as a sole carbon source, and targets a subset of PTS1 proteins (Effelsberg et al. 2016; Yifrach et al. 2016). Its substrates are Malate Synthase 1 (Mls1), Malate Synthase 2 (Mls2), and Glutathione Transferase Omega-like 1 (Gto1), all containing a classical PTS1 tripeptide (Effelsberg et al. 2016; Yifrach et al. 2016). We hypothesize that Pex9 enables priority targeting of these specific enzymes when it is expressed in oleate-containing medium since they are required in peroxisomes under fatty-acid-dependent growth. Hence Pex9 activity enables dynamic rewiring of peroxisomes in response to metabolic needs. But how does Pex9, a paralog of Pex5, recognize only a subset of PTS1 proteins, and what defines the targeting specificity of Pex9?

To better understand the targeting specificity of Pex9, we first looked for additional Pex9 cargos amongst the recently identified yeast peroxisomal proteins (Yifrach et al. 2021) and found one additional direct cargo. We used the known cargos to align the PTS1 and look for similar patterns. To verify the hypotheses that came up from this alignment, we performed site-directed mutagenesis on the PTS1 sequences of known Pex9 and Pex5 cargos and looked at their effect on Pex9-dependent targeting to peroxisomes and physical binding. In parallel, we modeled the PTS1-binding domain of Pex9 and Pex5 to identify distinguishing features of the binding cavity and the surrounding area of each cargo factor. Molecular dynamics simulations of Pex9- or Pex5-peptide complexes showed binding differences within the binding cavity. Finally, we performed an unbiased screen with variable PTS1 sequences to validate our findings of the properties that enable Pex9 recognition.

Using both the targeted approach as well as the unbiased screen, we found that Pex9 prefers hydrophobic and negatively charged residues upstream to the PTS1 tripeptide. In contrast, Pex5 was previously shown to prefer positively charged residues in these positions (DeLoache, Russ and Dueber 2016). This preference is supported by the model structures of the PTS1 binding domains, which showed that the PTS1 binding cavity of Pex9 is mostly hydrophobic and with positively charged patches in the surroundings, compared to the generally negative surface of Pex5. These distinct features highlight the complex and intricate targeting landscape of peroxisomes, which allows differential targeting enabling the peroxisome to rewire its function according to metabolic needs.

Results

Expanding the cargo range of Pex9 using a microscopy screen

To define motifs by aligning the PTS1 of Pex9 cargoes, it is important to have the biggest possible sample size. However, previous to this work only three Pex9 cargos were identified. Therefore, we sought to find additional proteins that can be targeted by Pex9. To this end, we performed a microscopic screen on a collection of ~40 yeast strains representing a set of recently identified yeast peroxisomal proteins (Yifrach et al. 2021), which were never tested for targeting by Pex9 (Figure 1A). All proteins in this collection harbor a Green Fluorescent Protein (GFP) tag at the amino terminus (N′) for visualization and to allow their C′ to be exposed in case they have a PTS1. To examine the dependence of the peroxisomal proteins on Pex9, we used an automated mating procedure to insert several genetic traits into each strain: I) a peroxisomal marker, Pex3-mCherry, II) a deletion of the main PTS1 targeting factor (*Δpex5*) and III) a constitutive expression of *PEX9* to enable visualization of its function in glucose-containing medium, as was done previously (Yifrach et al. 2016). We imaged the entire collection using a high content screening setup and looked for proteins that co-localize with peroxisomes when only Pex9 is expressed as a PTS1 targeting factor. Following analysis of all strains, we were able to identify two proteins that co-localized with peroxisomes in this condition – the Family of Serine Hydrolases 3 (Fsh3) protein, a newly identified peroxisomal lipase (Yifrach et al., 2021), and the Alpha-Factor Receptor regulator 1 (Afr1) protein, which is required for the formation of pheromone-induced projections in yeast (Konopka 1993) (Figure 1B).

To assess the capacity of Fsh3 and Afr1 to bind Pex9, we used a Yeast-2-hybrid (Y2H) assay. We found that Fsh3, but not Afr1, physically interacts with Pex9 (Figure 1C). The specific interaction between Pex9 and Fsh3 is suggested to

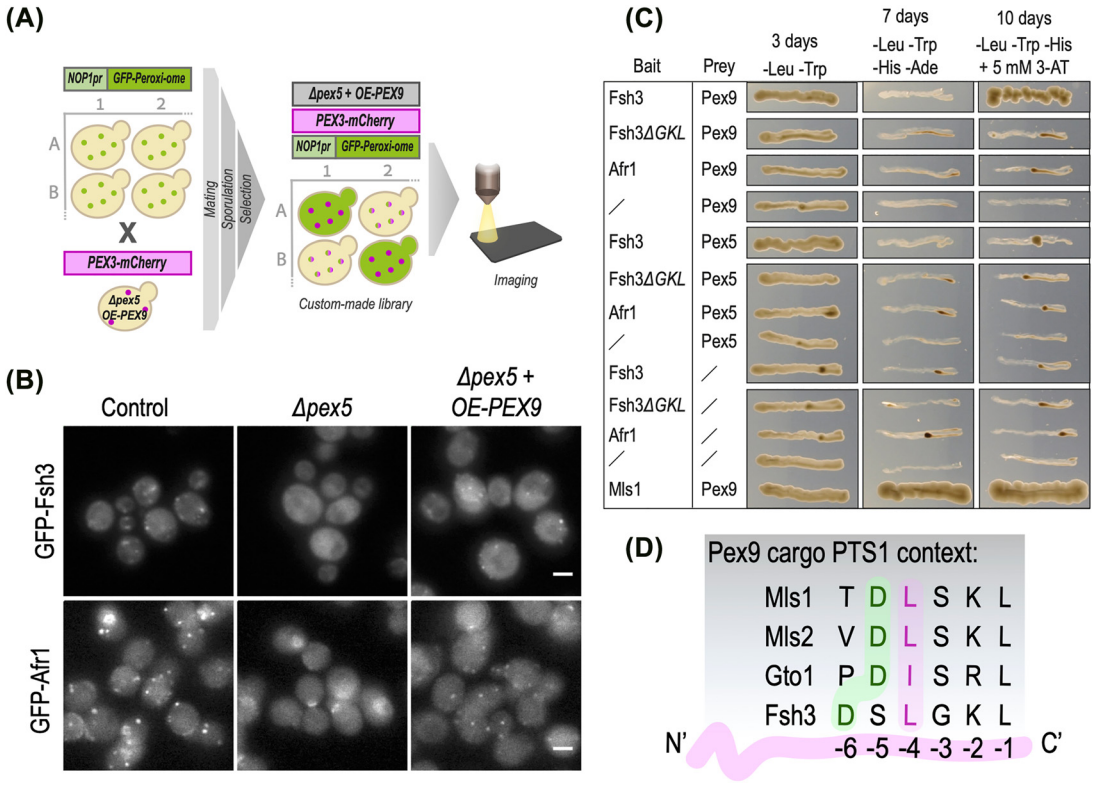

Figure 1: Expanding the cargo range of Pex9 using a microscopy screen and yeast 2-hybrid (Y2H) assays. (A) A query strain constitutively expressing Pex9 as the sole PTS1 targeting factor (*Δpex5* + TDH3pr-PEX9) and a peroxisomal marker (Pex3-mCherry) was used to genomically integrate these traits into a yeast N′ GFP collection of recently identified peroxisomal proteins (Yifrach et al. 2021) by utilizing an automated mating procedure. Then, fluorescence microscopy was applied to identify proteins that co-localize with the peroxisomal marker when the cells grew on media containing either glucose or oleate as the carbon source. (B) Fsh3 and Afr1 both co-localize with peroxisomes when Pex9 is constitutively expressed and *PEX5* is deleted, suggesting that they are newly identified cargos of Pex9. For all micrographs, a single focal plane is shown. The scale bar is 5 μm. (C) Y2H assays demonstrate that Fsh3 interacts with Pex9 in a PTS1-dependent manner, but Afr1 does not. (D) All Pex9-directed cargos show similar amino acid properties at positions −4 (hydrophobic residue L or I) and a negatively charged residue D in position -5 or -6 from the C′ of the protein.

be comparably weak or that Fsh3 abundance is low. This is demonstrated by colony formation, which takes up to ten days on a medium that contains adenine and 5 mM 3-amino triazole (3-AT) (for more information on this assay see materials and methods). Afr1 does not contain a canonical PTS1 at its C' (the last six amino acids of the protein are FTHYLI), which altogether suggests that Afr1 may rely indirectly on Pex9. For example it could piggyback on another Pex9 cargo that contains a PTS1 similarly to a previously shown Pex5 cargo (Gabay-Maskit et al. 2020). Despite being weak, the binding of Fsh3 to Pex9 does depend on the PTS1 tripeptide of Fsh3 (Figure 1C). Put together, this suggests that Fsh3 is an additional direct cargo for Pex9. Interestingly, in the Y2H assay, neither Fsh3 nor Afr1 interacted with Pex5. This was unexpected since the microscopy analysis showed a reduction in peroxisomal localization for both proteins following the deletion of *PEX5*. This discrepancy between the two assays suggests that the Y2H is less sensitive than the microscopy assay.

After we expanded our cargo list, we could better assess unique sequence features. We compared the context of the PTS1 (the amino acids upstream to the PTS1 tripeptide) of the four Pex9 cargos Mls1, Mls2, Gto1, and Fsh3 (Figure 1D). We noticed that all cargos have a hydrophobic residue one amino acid upstream to the tripeptide (position −4 from the C′) and a negatively charged residue in position −5 or −6 from the C'. This similarity suggests that these features are important for recognition by Pex9.

Mutagenesis in the PTS1 context of known cargos uncovers Pex9 determinants

To explore whether the negatively charged residue in the PTS1 context of the Pex9 cargos plays an important role in their recognition, we substituted the charged residues at this position in various cargo proteins and looked for changes in the targeting ability. To visualize the effect of

the PTS1 context, we constructed an integration plasmid containing a GFP fused at its C′ to the last 10 amino acids of Fsh3. We transformed this construct into the genome of a strain that constitutively expresses only Pex9, but not Pex5 (*Δpex5 + TDH3pr-PEX9*). We validated that the PTS1 motif of Fsh3 is sufficient to target the GFP to peroxisomes by Pex9 (Figure 2A, wtPTS1). Then, we mutated the negatively charged residue aspartate (D) in position −6 of the C′ to A, which has no charge. We indeed observed a reduction, but not a complete loss, of the peroxisomal localization of the protein (Figure 2A, D(-6)A).

Furthermore, when we performed Y2H assays and mutated the D to a positively charged residue, K, it obliterated the interaction of Fsh3 with Pex9 (Figure 2B). However, when we mutated the D to K in the other cargos Mls1 and Mls2, the proteins could still interact with Pex9. These data suggest that the negatively charged residue in position −6 or −5 of the PTS1 plays a role in some cargo proteins but is not the sole nor definitive determinant for Pex9 cargo recognition.

Since factor-specific targeting requires that a cargo both binds Pex9 with enhanced affinity and that it binds Pex5 with reduced affinity, we also assayed the effect of the above-mentioned mutations on Pex5 binding. Interestingly, while the wild-type Mls1 and Mls2 (harboring a D at position −5) did not interact with Pex5, the D to K exchange in Mls1 and Mls2 promoted the interaction with Pex5 (Figure S1). These observations are in agreement with previous data showing that positively charged residues in the PTS1 context enhance targeting by Pex5 (DeLoache, Russ and Dueber 2016). We speculate that the D in position −5 or −6 of the Pex9 cargos serves to reduce capture by Pex5, rather than to enhance the binding to Pex9.

Next, we tested whether a mutation closer to the PTS1 tripeptide affects the targeting ability of Pex9. We changed S to A in position −5 of Fsh3 and checked how well the GFP-PTS1 (last 10aa of Fsh3) localizes to peroxisomes. Although the basal targeting of the native PTS1 construct was already quite good, we were able to observe moderately-

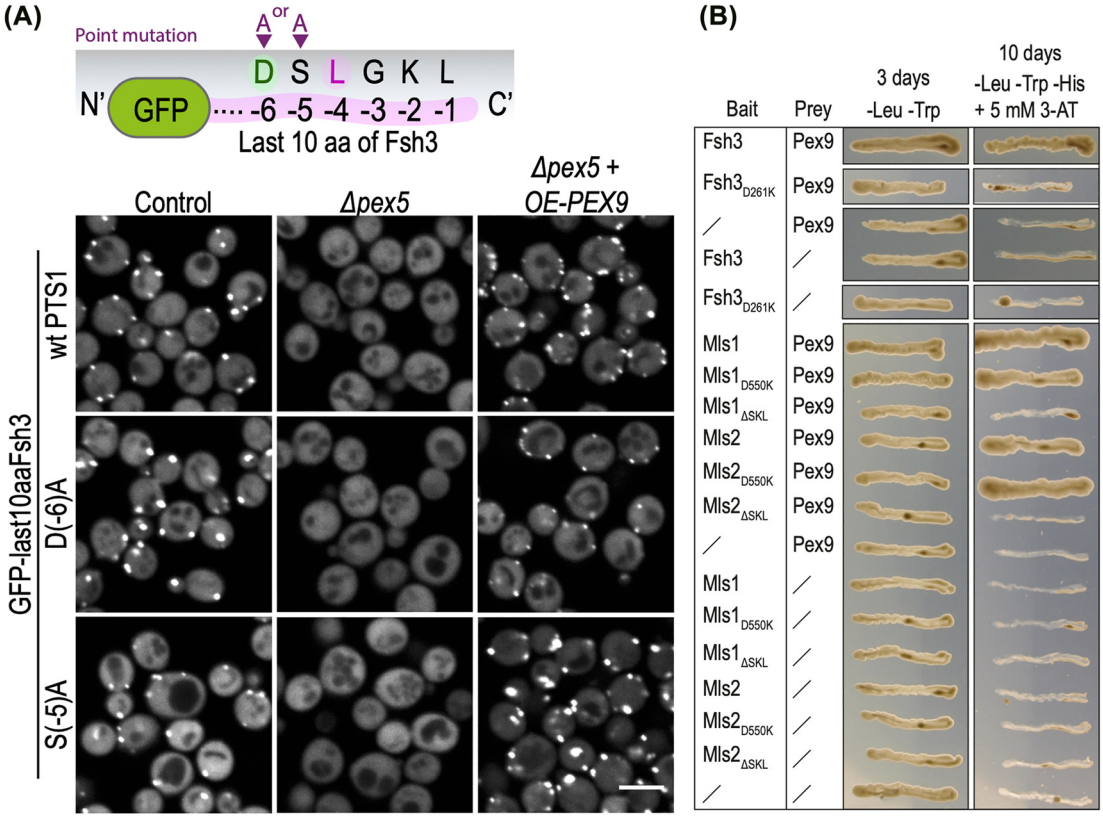

Figure 2: Mutagenesis in the PTS1 context of known cargos uncovers Pex9 determinants. (A) Directed point mutagenesis was applied on an integration plasmid containing a GFP fused at its C′ to the last 10 amino acids of Fsh3 to substitute position −6 or −5 from aspartic acid (D) or serine (S) to alanine (A). While the substitution of D to A at position −6 showed reduced GFP localization to peroxisomes, the S to A substitution at position −5 showed moderately enhanced GFP localization in peroxisomes when the cells express Pex9 as the sole PTS1 targeting factor. For all micrographs, a single focal plane is shown. The scale bar is 5 µm. (B) Y2H assays show that a D to lysine (K) substitution in the PTS1 context of Fsh3 obliterates the interaction with Pex9, but a similar substitution of D to K in Mls1 and Mls2 does not affect the interaction with Pex9, suggesting that D in the context of the PTS1 is not the sole nor definitive determinant for Pex9 cargo recognition.

enhanced peroxisomal localization (which we define as targeting) in the mutated construct compared to the WT PTS1 (Figure 2A, S(-5)A). S is a polar amino acid, while A is non-polar. This suggests that Pex9 prefers a non-polar amino acid at a position closer to the PTS1 tripeptide.

Exploring Pex9 targeting specificity using natural non-binders

Intrigued by the ability to enhance import by Pex9, we decided to mutate the PTS1 motifs of a cargo protein that does not normally use Pex9 to potentially induce import (non-binders). We reasoned that this would facilitate visualization as there will be a sudden gain of targeting from no initial targeting. To start with a Pex9 non-binding PTS1, we first tested the last ten amino acids of several proteins whose full-length version is Pex9 independent (they are not localized to peroxisomes when Pex9 is expressed and Pex5 is absent). We focused on three cargo proteins with a high priority to Pex5, Malate Dehydrogenase 3 (Mdh3), Carnitine Acetyltransferase 2 (Cat2), and Lysine requiring 1 (Lys1) (Rosenthal et al. 2020), and fused their last ten amino acids to the C′ of a GFP. Then, we integrated these constructs into an inert locus in the yeast genome. While the full-length proteins are not Pex9 cargos (Figure S2 and (Yifrach et al. 2016), surprisingly, we found that the fusion of only the last ten amino acids of both Mdh3 and Cat2 was sufficient to co-localize GFP to peroxisomes in a Pex9-dependent manner (Figure 3A and B). We used a Y2H assay to validate the microscopy-based observation and showed that indeed the full-length Mdh3 does not interact with Pex9, while a peptide consisting of only the last ten amino acids of Mdh3 does (Figure 3C). Conversely, we found that the full-length Pex9 cargos, Fsh3, and Mls1, do not interact with Pex5 in Y2H, but peptides consisting of only their last ten amino acids do (Figure 3C). This striking observation suggests that additional domains in the full protein prevent, or reduce, the interaction with both Pex5 and Pex9 and block targeting even when the PTS1 by itself could enable binding.

We continued to work on the last ten amino acids of Lys1, which were not sufficient to mediate Pex9-dependent targeting (Figure 3D, upper panel). To enhance Pex9 binding, we replaced the amino acids at positions –5 and –4 with the negatively charged residue D and a non-polar residue L, either alone or in combination. While the D mutation had no visible effect on the localization of the GFP, the peptide with the L mutation showed a weak peroxisomal signal, demonstrating that a single amino acid change to a non-polar residue at position –4 is sufficient to allow targeting by Pex9.

Overall, our data imply that the PTS1 targeting specificity of Pex9 is largely dependent on the presence of a non-polar, hydrophobic residue flanking the PTS1 tripeptide. Moreover, we suggest that the negatively charged residue at positions –5 or –6 of the PTS1 has two roles – to enhance the binding of specific cargo proteins to Pex9 and to prevent binding to Pex5.

Pex9 molecular modeling support hydrophobicity in the PTS1 binding area as a major determinant of Pex9 binding

Our targeted approach highlighted the preference of Pex9 for a hydrophobic residue preceding the PTS1 tripeptide. This distinguishes Pex9 from Pex5, which is known to prefer positively charged residues in this context (DeLoache, Russ and Dueber 2016). To uncover the structural features that differentiate the two targeting factors in their binding preference, we constructed a model structure of the Pex9 PTS1-binding domain in a similar manner to the modeling of Pex5 that we described previously (Gabay-Maskit et al. 2020) (Figure 4A). The models highlight that the Pex5 surface around the PTS1-binding cavity has large negative electrostatic potential patches (red), while the surface of the cognate Pex9 regions appears more hydrophobic (white). This is especially obvious for the shallow cavity that binds the amino acid in position –2 (black arrows) and the bottom of the PTS1 binding cavity (Figure 4A). In addition, Pex9 has several positive electrostatic patches (blue) at the edge of the peptide-binding cavity.

We then performed Molecular Dynamics (MD) simulations of a cargo factor (Pex5 or Pex9) with peptides consisting of six C′ amino acids of four PTS1 proteins that are Pex9 cargo: Mls1, Mls2, Gto1, and Fsh3. We previously showed that the binding stability of a peptide to Pex5 could be estimated from the constancy of hydrogen bonds (H-bonds) between peptide backbone atoms and specific Pex5 residues, particularly H-bonds of peptide residues –1 and –3 (Yifrach et al. 2021). The Pex5 residues that form these H-bonds are conserved between Pex5 and Pex9 supporting the importance of the C′ tripeptide for binding. The context residues, however, behaved differently in the simulations for Pex5 and Pex9 complexes. In the starting structures of all the complexes, the side chain of peptide residue –4 pointed outwards, making either no, or little, contact with the cargo factor, as seen in the experimental structure that was used as the modeling template (Gatto et al. 2000). While in the Pex5 simulations this side chain remained mostly exposed, in the Pex9 simulations the peptide changed conformation within 50–100 ns

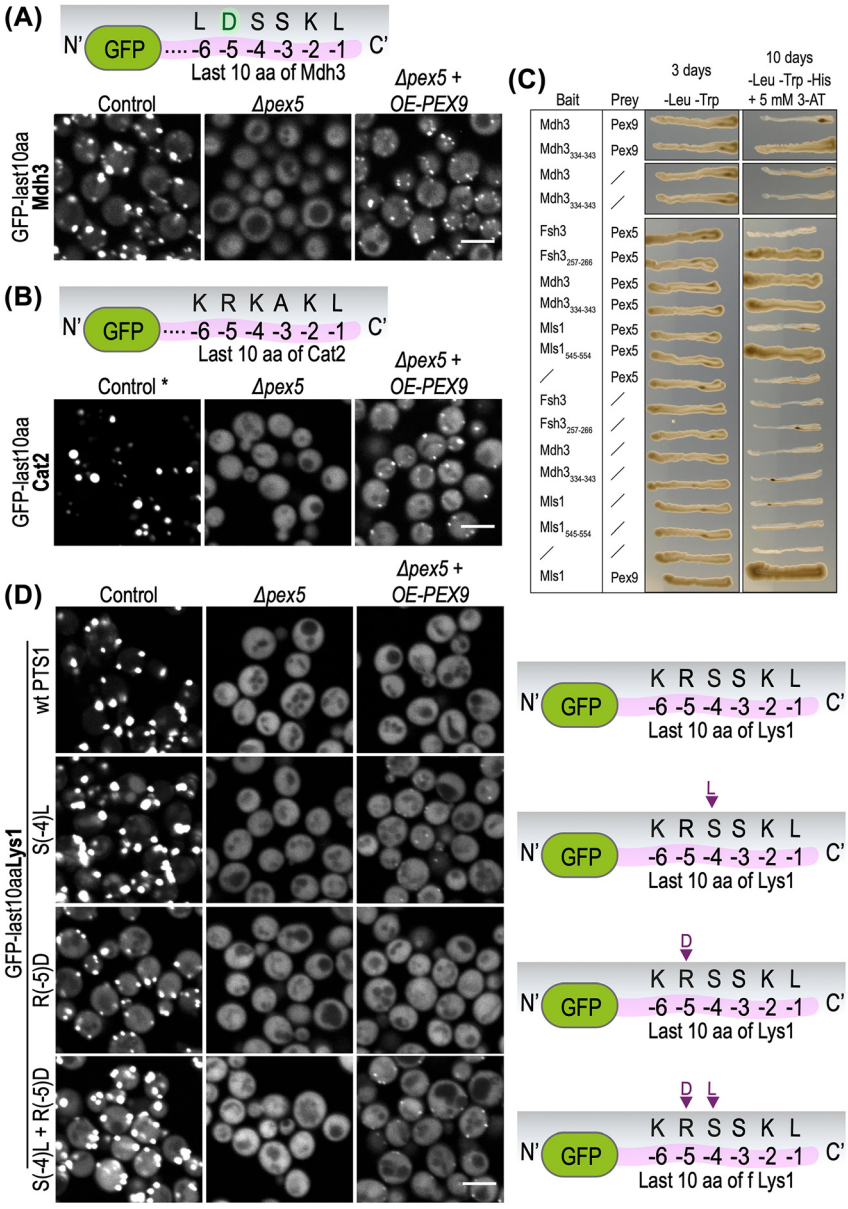

Figure 3: Exploring Pex9 targeting specificity using natural non-binders. Integration plasmids containing a GFP fused at its C′ to the last 10 amino acids of (A) Mdh3 or (B) Cat2, show that the last 10 amino acids of both Mdh3 and Cat2 were sufficient to co-localize the GFP to peroxisomes in a Pex9-dependent manner, although the full-length proteins are not cargos of Pex9. The asterisk indicates that GFP-last 10aaCat2 Control (in B) had a higher signal compared to the other images in the panel, hence a different image contrast was used. (C) Y2H assays validate that the last 10 amino acids of Mdh3 (aa334–343) can interact with Pex9 despite the fact that the full-length protein does not. Similarly, the last 10 amino acids of the Pex9 cargos Fsh3 (aa257–266) and Mls1 (aa545–554) interact with Pex5, more strongly than the full-length proteins. This suggests that additional parameters in the full protein prevent, or reduce, the interaction with the inappropriate targeting factor. (D) An integration plasmid containing a GFP fused at its C′ to the last 10 amino acids of Lys1 shows that the native PTS1 of Lys1 was not sufficient to co-localize the GFP to peroxisomes in a Pex9-dependent manner. Directed mutagenesis substitution of positions −5 and −4 to the negatively charged residue D and/or a non-polar residue leucine (L) show that the L mutation enabled a weak GFP peroxisomal localization, demonstrating that a single non-polar residue at position −4 is sufficient to mediate Pex9 specificity. For all micrographs, a single focal plane is shown. The scale bar is 5 μm.

and the sidechain of its −4 residue pointed toward the bottom of the PTS1 binding cavity (Figure 4B and Figure S3). This hydrophobic sidechain (L or isoleucine (I)) made tight contacts with hydrophobic Pex9 residues that replace more polar residues of Pex5 (e.g. tyrosine (Y) 410, and A437 in Pex9 versus S507 and S534 in Pex5). Together with additional residues, they form a more hydrophobic surface at the entrance to the peptide-binding cavity of Pex9 and form

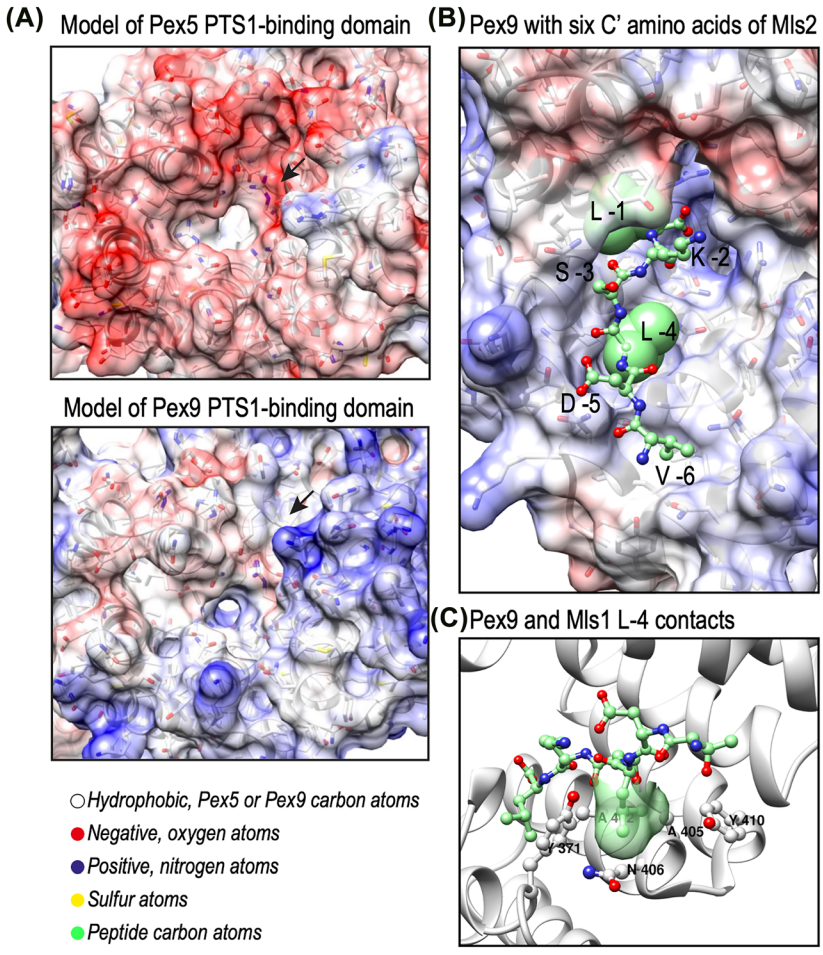

Figure 4: Pex9 molecular modeling support hydrophobicity in the PTS1 binding area as a major determinant of Pex9 binding. (A) Molecular modeling of the PTS1 binding domains of Pex9 and Pex5 indicates that the Pex5 surface around the PTS1 binding cavity has large negative electrostatic potential patches (red), while the surrounding area of the PTS1 cavity of the cognate Pex9 regions appears mostly hydrophobic (white) with several positive electrostatic patches (blue) at the edge of the peptide-binding cavity. Black arrows point to the shallow cavity that binds peptide residue −2. (B) Molecular dynamics simulations of complexes of Pex9 with peptides consisting of six C′ amino acids of the known Pex9 cargo Mls2 show that the sidechain of the peptide's −4 residue points toward the bottom of the PTS1 binding cavity and makes tight contacts with hydrophobic Pex9 residues (all other Pex9 cargo behaved in the same manner). (C) A detailed snapshot from the simulations depicts the contacts between Pex9 residues and the Mls1 L-4 sidechain. Legend for atom coloring on the bottom left.

hydrophobic contacts with L or I at position −4 of Pex9 cargos (Figure 4C). These results strongly support the notion that Pex9 cargos are selected by the hydrophobic residue in position −4 of the PTS1.

A systematic screen shows a correlation between Pex9-dependent peroxisomal localization and hydrophobicity of residue −4 of PTS1 sequences

To validate our findings in an unbiased manner and to investigate more variations of the PTS1 context that may favor Pex9, we took advantage of a library of integration plasmids containing randomized sequences preceding the canonical PTS1 tripeptide S-K-L residues (DeLoache, Russ and Dueber 2016). This library was previously used to find the optimal Pex5 cargo sequence–the enhanced PTS1 import sequence. Each integration plasmid in this pooled library contains a Yellow Fluorescent Protein (YFP) linked at its C′ to a variable sequence of six amino acids (XXXXXX) preceding the SKL tripeptide. We genomically integrated this YFP-XXXXXX-SKL library into a strain constitutively expressing Pex9 as the sole PTS1 targeting factor and picked single colonies into an arrayed format (Figure 5A). Then, we imaged each strain and sequenced the contained plasmid to match the ratio of the YFP-XXXXXX-SKL peroxisome/cytosol localization to the identity of the variable amino acid

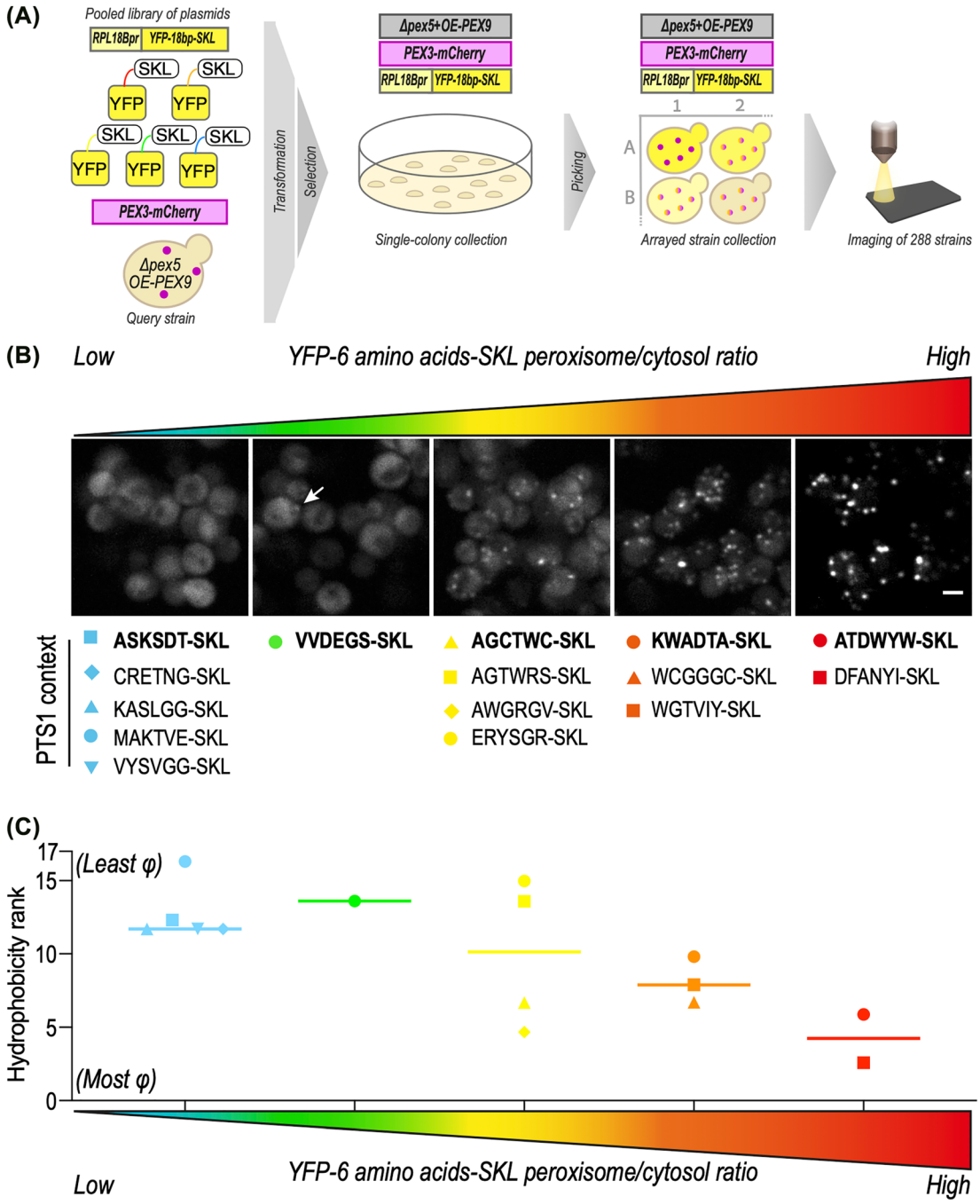

Figure 5: A systematic screen shows a correlation between Pex9-dependent peroxisomal localization and hydrophobicity of residue −4 of PTS1 sequences. (A) A pooled library of plasmids containing YFP fused to a stretch of six random amino acids followed by the tripeptide SKL was transformed into a strain constitutively expressing Pex9 as the sole PTS1 targeting factor (*Δpex5* + *TDH3pr-PEX9*) and a peroxisomal marker (Pex3-mCherry). Cells from single colonies were imaged and the PTS1 context of each plasmid was sequenced. (B) Fifteen distinct PTS1 context sequences (the random stretches) were identified and matched to the peroxisome/cytosol localization ratio of their cognate YFP construct. The white arrow is pointing at a peroxisome. For all micrographs, a single focal plane is shown. The scale bar is 5 μm. (C) Amino acid analysis shows that the YFP peroxisome/cytosol localization ratio correlates with the hydrophobicity score of the residue at position −4 from the C′ of each construct. This combined hydrophobicity rank (Trinquier and Sanejouand 1998) gives low values for hydrophobic residues (most φ) and high values for hydrophilic residues (least φ). The analysis supports our hypothesis that Pex9 cargos are selected by the hydrophobic residue in position −4 of the PTS1.

sequence. We found a wide range of peroxisome/cytosol localization ratios, from very high to very low. Despite redundancy in sequences, we could retrieve 15 distinct linkers that correspond to the wide range of phenotypes (Figure 5B). We manually validated two sequences from the screen by fusing them to the C′ of GFP (Figure S4). We looked for potential determinants in the variable sequences that will explain the different peroxisome/cytosol localization ratios. We tested the various positions as well as many size/hydrophobicity/charge aspects. The best correlation was achieved when the peroxisome/cytosol ratio was plotted against the hydrophobicity score of the residues at position −4 (Figure 5C). The hydrophobicity scores were taken from an averaged scale built from 43 different hydrophobicity studies (Trinquier and Sanejouand 1998), and gave the best correlation relative to any singular hydrophobicity scale examined. The analysis validates our hypothesis that Pex9 cargos are selected by the hydrophobic residue in position −4 of the PTS1.

Discussion

'Being in the right place at the right time' is not simply a motto – when it comes to cellular proteins, it is an absolute necessity. In a cell, the right proteins must be shuttled from the cytosol to their destination compartment upon demand. When *Saccharomyces cerevisiae* cells rely on fatty acid-containing media, peroxisomes become essential, as they are the sole organelles that break down fatty acids in baker's yeast. Thus, peroxisomes must dynamically change their protein content according to the cell's metabolic needs. To give targeting priority to central catabolic enzymes, the metabolically regulated arm of the targeting machinery is activated. Both the targeting factor Pex9 and the Pex7 co-factor, Pex18, are upregulated to boost the targeting of specific PTS1 and PTS2 proteins, respectively (Effelsberg et al., 2015, 2016). Although Pex9 is a paralog of Pex5, it targets a specific subset of Pex5 cargo proteins – Mls1, Mls2, Fsh3, and Gto1. These enzymes are especially needed in peroxisomes during oleate-dependent growth. The malate synthases are targeted to peroxisomes to participate in the glyoxylate cycle, which generates four-carbon molecules (such as malate) by utilizing the β-oxidation product, acetyl-CoA (Kunze et al. 2002). The glutathione transferase Gto1 protects peroxisomes from oxidative stress that is generated during the course of β-oxidation (Barreto et al. 2006). Fsh3, which we identified as a Pex9 cargo in this work, was recently suggested to be a lipase (Yifrach et al. 2021) whose function should be further studied.

How is the binding specificity achieved? Binding specificity is a function of both positive and negative selection, meaning the binding to one specific partner while *not* binding to others (Schreiber and Keating 2011). Indeed, our work shows that some residues, such as the −5/-6 negative charge upstream of the PTS1 tripeptide, can act to either enhance binding to Pex9, weaken binding to Pex5, or both. Our modeling results suggest that this is achieved by long-range electrostatic screening. An example of such a mechanism was recently brought forward by a study on the selectivity of the Golgi to Endoplasmic Reticulum (ER) retrieval signals showing that the KDEL receptors use a charge screening mechanism to differentiate between their cognate signals (Gerondopoulos et al. 2021): the charge distribution across the surface of the KDEL receptor is used as an "antenna" for the initial signal capture and proofreading. We argue that an "antenna" like mechanism exists also for Pex5 and Pex9. Indeed, we observed that the electrostatic properties on the surfaces of the PTS1-binding cavities of Pex5 and Pex9 are significantly different. The surface of Pex5 has large negative electrostatic potential patches within and around the protein-binding cavity, while Pex9 in this region is mostly hydrophobic with several positive electrostatic patches at the edge of the binding cavity. We found that while the PTS1 motifs of non-binders can drive the targeting of GFP to peroxisomes, the full-length proteins are not interacting with the respective targeting factor, Pex5 or Pex9, in Y2H assays. This suggests that interaction interfaces outside of the PTS1 motif binding cavity significantly contribute to the binding specificity. These binding interfaces can either attract the proteins to their cognate targeting factor and/or repulse interaction with the inappropriate targeting factor at the initial stage of cargo protein screening.

In addition, the properties of the PTS1 tripeptide itself and the preceding amino acids contribute to this positive and negative selection. We show by molecular modeling, a targeted experimental approach, and an unbiased screen, that the amino acid at position −4 of the PTS1 has the most significant effect on binding selectivity by Pex9. The replacement of only a few residues from polar in Pex5 to hydrophobic in Pex9 forms a more hydrophobic region at the entrance to the peptide-binding cavity. Correspondingly, all Pex9 cargos contain a hydrophobic residue at position −4.

Our work exemplifies how changes in the binding cavity of two rather similar targeting factors lead to different cargo binding specificities. These findings expand the range of capabilities of how peroxisomes achieve exquisite targeting specificity – from the presence of multiple differentially regulated parallel pathways for targeting, through affinity-tuning of various PTS1s to provide priority targeting

(Rosenthal et al. 2020). Each cargo has a unique targeting propensity that can also be regulated to enable the dynamic rewiring of protein content in peroxisomes upon demand and shows the beauty and complexity of the peroxisomal targeting machinery.

Materials and methods

Yeast strains and strain construction

All strains in this study are based on the BY4741 laboratory strain (Brachmann et al. 1998) except for the PJ69-4a that were used for the Y2H assays (James et al. 1996). See the complete list of yeast strains and primers in Table S1. Cells were genetically manipulated using a transformation method that includes the usage of lithium-acetate, polyethylene glycol, and single-stranded DNA (Daniel Gietz and Woods 2002). A pYM-based plasmid (Janke et al. 2004) was modified to contain the last 10 aa of different PTS1 proteins at the C′ of the GFP sequence. Point mutations were introduced using restriction-free cloning. Plasmids are described in Table S2. Constructs were genomically integrated into the HO locus in strains containing Pex3-mCherry, with or without *pex5* deletion and constitutive *PEX9* expression. Primers for validation of correct insertion were designed using the Primers-4-Yeast website (Yofe and Schuldiner 2014).

Yeast growth media

Synthetic media used in this study contains 6.7 g/L yeast nitrogen base with ammonium sulfate (Conda Pronadisa #1545) and 2% glucose, with complete amino acid mix (oMM composition, Hanscho et al. 2012), unless written otherwise. When Hygromycin or Geneticin antibiotics were used, media contained 0.17 g/L yeast nitrogen base without ammonium sulfate (Conda Pronadisa #1553) and 1 g/L of monosodium glutamic acid (Sigma-Aldrich #G1626) instead of yeast nitrogen base with ammonium sulfate. When mentioned, 500 mg/L Hygromycin B (Formedium), 500 mg/L Geneticin (G418) (Formedium), and 200 mg/L Nourseothricin (Silcol Scientific Equipment LTD) were used.

Yeast library preparation using a synthetic genetic array (SGA)

To create collections of haploid strains containing GFP-tagged proteins with additional genomic modification (i.e. Pex3-mCherry (a peroxisomal marker), *PEX5* deletion (*Δpex5*), and *PEX9* constitutive-expression (*TDH3pr-PEX9*)), a query strain was constructed based on an SGA compatible strain (for further information see Table S1). Using the SGA method (Cohen and Schuldiner 2011; Tong and Boone 2006) the query strain was crossed with a collection of strains from the SWAT N′-GFP library (Yofe et al. 2016; Weill et al. 2018) containing ~40 strains of recently-identified peroxisomal proteins (Yifrach et al. 2021) together with controls. To perform the SGA in an arrayed format, we used a RoToR benchtop colony arrayer (Singer Instruments). In short: mating was performed on rich medium plates, and selection for diploid cells was performed on SD-URA plates containing Nourseothricin, Hygromycin, and Geneticin antibiotics. Sporulation was induced by transferring cells to nitrogen starvation media plates for 7 days. Haploid cells containing the desired mutations were selected by transferring cells to SD-URA plates containing the same antibiotics as for selecting diploid cells, alongside the toxic amino acid derivatives 50 mg/L Canavanine (Sigma-Aldrich) and 50 mg/L Thialysine (Sigma-Aldrich) to select against remaining diploids, and lacking Histidine to select for spores with an A mating type.

Yeast library preparation from a library of pooled plasmids

A library of pooled Venus-PTS1 plasmids (DeLoache, Russ and Dueber 2016) was transformed genomically into a strain containing Pex3-mCherry as a peroxisomal marker, *Δpex5*, and *TDH3pr-PEX9*. 288 single colonies were picked to a 384-well plate containing SD-URA liquid media supplemented with Nourseothricin, Hygromycin, and Geneticin for selection. Then, the collected strains were imaged using automated fluorescence microscopy. In parallel, the DNA of each strain was extracted by dissolving in 20 mM NaOH followed by boiling at 95 °C for 20 min in a PCR machine. Then, a 270 bp DNA containing the variable PTS1 region was amplified using a PCR reaction with appropriate primers (F–cgaaaagagagatcacatgg, R–gaaagcaacctgacctacag). The amplified DNA was cleaned using a GenElute 96 Well PCR Clean-up kit (Sigma-Aldrich) and sent for sequencing.

Automated fluorescence microscopy

The collections (~40 strains of NOP1pr-GFP-recently identified peroxisomal proteins, Figure 1 and 288 strains with YFP-XXXXXX-SKL, Figure 5) were visualized using an automated microscopy setup: cells were transferred from agar plates into 384-well polystyrene plates for growth in liquid media using manual handling. Liquid cultures were grown in a LiCONiC incubator, overnight at 30 °C in an SD-URA medium. An EVO freedom liquid handler (TECAN) connected to the incubator was used to dilute the strains to an OD_{600} of ~0.2 into plates containing SD medium (6.7 g/L yeast nitrogen base and 2% glucose) supplemented with –URA amino acids. For the ~40 NOP1pr-GFP strains we performed an additional screen in S-oleate (6.7 g/L yeast nitrogen base, 0.2% oleic acid, and 0.1% Tween-80) supplemented with –URA amino acids. Plates were incubated at 30 °C for 4 h in SD medium or for 20 h in S-oleate. The cultures in the plates were then transferred by the liquid handler into glass-bottom 384-well microscope plates (Matrical Bioscience) coated with Concanavalin A (Sigma-Aldrich). After 20 min, wells were washed twice with SD-Riboflavin complete medium (for screens in glucose) or with double-distilled water (for the screen in oleate) to reduce autofluorescence, remove non-adherent cells, and obtain a cell monolayer. The plates were then transferred to the ScanR automated inverted fluorescence microscope system (Olympus) using a robotic swap arm (Peak Robotics). Images of cells in the 384-well plates were recorded in the same liquid as the washing step at 24 °C using a 60× air lens (NA 0.9) and with an ORCA-flash 4.0 digital camera (Hamamatsu). Images were acquired in two channels: YFP (excitation at 488 nm, emission filter 525/50 nm) and mCherry (excitation at 561 nm, emission filter 617/73 nm). Image analysis was performed manually using ImageJ software.

Manual microscopy

Manual microscopy imaging was performed for strains with NOP1pr-GFP-last 10 aa of Fsh3 (Figure 2) Mdh3, Cat2, and Lys1 (Figure 3). Yeast strains were grown as described above for the high-throughput microscopy with changes in the selection required for each strain (see yeast strain information in Table S1). Imaging was performed using the VisiScope Confocal Cell Explorer system, composed of a Zeiss Yokogawa spinning disk scanning unit (CSU-W1) coupled with an inverted Olympus microscope (IX83; x60 oil objective; Excitation wavelength of 488 nm for GFP). Images were taken by a connected PCO-Edge sCMOS camera controlled by VisView software.

Yeast two-hybrid assay to assess protein-protein interactions

PJ69-4A cells (James, Halladay and Craig 1996) were transformed with plasmids derived from pPC86 (GAL4-activation domain, AD ('Prey')) and pPC97 (GAL4-DNA-binding domain, BD ('Bait')) (Chevray and Nathans 1992; Kerssen et al. 2006), containing genes encoding proteins of interest. Transformed cells were selected on YNBG (0.17% [w/v] yeast nitrogen base without amino acids, 0.5% [w/v] ammonium sulfate, amino acids according to auxotrophic requirements, pH 6.0) plates lacking leucine (leu) and tryptophan (trp) containing 2% [w/v] glucose (YNBG). Clones were streaked onto YNBG-trp-leu (control), YNBG -trp-leu-his-ade, and/or YNBG -trp-leu-his + 5 mM 3-amino triazole (3-AT) plates and incubated for 3, 7, or 10 days at 30 °C, respectively. The reporter genes HIS3 and ADE2 are under the control of GAL1 or GAL2 promoters, respectively. Thus, they are only expressed when Gal4-AD and Gal4-BD of the bait and prey fusion proteins are in close proximity due to protein-protein interaction. Since the absence of adenine is a very stringent selection condition (James, Halladay and Craig 1996), weak interactions were investigated in the presence of adenine. However, to suppress unspecific leakage of the growth phenotype upon longer incubation on plates lacking histidine, the competitive His3-inhibitor 3-AT was added to avoid false-positive results. Overall, the addition of 3-AT and longer incubation times, when compared to the control plates, were chosen to visualize weak protein-protein interactions by cell growth on plates lacking histidine or adenine.

Molecular modeling and molecular dynamics (MD) simulations

Model structures of Pex9's TPR (PTS1 binding) domain, residues 287–484, with bound 6 amino-acid peptides were constructed based on the experimental structures of human Pex5 complexes. The sequence identity for the TPR domain was only 29% to the human Pex5 TPR domain structure in Gatto et al. 2000 (PDB entry 1FCH) but it was spread along the whole sequence. The starting model of yeast Pex9 was constructed using Modeller (Šali and Blundell 1993) as implemented in UCSF-Chimera (Pettersen et al. 2004). The position of the cargo peptide in the starting models was based on the structure of human Pex5-peptide complex 1FCH. As a result, the sidechain of residue −4 of the peptide pointed away from and made no direct contacts with Pex9. We explored the stability of the Pex9/peptide complexes using molecular dynamics. Each starting model was immersed in a box of water, neutralized and energy minimized. Two trajectories of 300 ns each were calculated for every model complex, and frames were extracted at 5 ns intervals and inspected manually. MD simulations were executed with the Gromacs package (Van Der Spoel et al. 2005). The minimum distance between peptide and Pex9 residues was calculated using the Gromacs package analysis options. UCSF-chimera was used to visualize frames from the Pex9/peptide trajectories and to produce Figure 4.

Acknowledgments: We would like to thank Prof. John Dueber for sharing the library of pooled Venus-PTS1 plasmids with us.

Author contributions: EY, MR, and LDCZ performed the experiments; ME performed the molecular modeling and molecular dynamics simulations and analyses; EY and ZG performed the microscopy screens; AT and YP generated all the plasmids that were used for the Pex9 targeting assay using microscopy; MK contributed to conceptualizing the initial work; WS, RE, MS, and EZ supervised the work; EY, MR, WS, RE, MS, and EZ wrote the manuscript; All authors read and gave feedback on the manuscript.

Research funding: Work in the Schuldiner lab is supported by the ERC CoG OnTarget (864068) and Israeli Science Foundation grants 760/17 and 914/22. The robotic system of the Schuldiner lab was purchased through the kind support of the Blythe Brenden-Mann Foundation. MS is an Incumbent of the Dr. Gilbert Omenn and Martha Darling Professorial Chair in Molecular Genetics. RE is supported by a grant of the Deutsche Forschungsgemeinschaft (FOR1905). EY is supported by the Ariane de Rothschild Women Doctoral Program. RE, and LDCZ are supported by grants from the Marie Curie Initial Training Networks (from the European Commission, PerICo 812968, and PerFuMe 316723) and MS is supported by PerICo 812968.

Conflict of interest statement: The authors declare no competing interests.

References

Aviram, N. and Schuldiner, M. (2017). Targeting and translocation of proteins to the endoplasmic reticulum at a glance. J. Cell Sci. 130: 4079–4085.

Barreto, L., Garcerá, A., Jansson, K., Sunnerhagen, P., and Herrero, E. (2006). A peroxisomal glutathione transferase of *Saccharomyces cerevisiae* is functionally related to sulfur amino acid metabolism. Eukaryot. Cell 5: 1748–1759.

Brachmann, C.B., Davies, A., Cost, G.J., Caputo, E., Li, J., Hieter, P., and Boeke, J.D. (1998). Designer deletion strains derived from *Saccharomyces cerevisiae* S288C: a useful set of strains and plasmids for PCR-mediated gene disruption and other applications. Yeast 14: 115–132.

Brocard, C. and Hartig, A. (2006). Peroxisome targeting signal 1: is it really a simple tripeptide? Biochim. Biophys. Acta. Mol. Cell Res. 1763: 1565–1573.

Chevray, P.M. and Nathans, D. (1992). Protein interaction cloning in yeast: identification of mammalian proteins that react with the leucine zipper of Jun. Proc. Natl. Acad. Sci. U.S.A. 89: 5789–5793.

Cohen, Y. and Schuldiner, M. (2011). Advanced methods for high-throughput microscopy screening of genetically modified yeast libraries. Methods Mol. Biol. 781: 127–159.

Daniel Gietz, R. and Woods, R.A. (2002). Transformation of yeast by lithium acetate/single-stranded carrier DNA/polyethylene glycol method. In: Guthrie, C. and Fink, G.R. (Eds.), *Guide to yeast genetics and molecular and cell biology - Part B*. Academic Press, p. 87–96.

DeLoache, W.C., Russ, Z.N., and Dueber, J.E. (2016). Towards repurposing the yeast peroxisome for compartmentalizing heterologous metabolic pathways. Nat. Commun. 7: 11152.

Effelsberg, D., Cruz-Zaragoza, L.D., Tonillo, J., Schliebs, W., and Erdmann, R. (2015). Role of Pex21p for piggyback import of Gpd1p and Pnc1p into peroxisomes of *Saccharomyces cerevisiae*. J. Biol. Chem. 290: 25333–25342.

Effelsberg, D., Cruz-Zaragoza, L.D., Schliebs, W., and Erdmann, R. (2016). Pex9p is a new yeast peroxisomal import receptor for PTS1-containing proteins. J. Cell Sci. 129: 4057–4066.

Fodor, K., Wolf, J., Erdmann, R., Schliebs, W., and Wilmanns, M. (2012). Molecular requirements for peroxisomal targeting of alanine-glyoxylate aminotransferase as an essential determinant in primary hyperoxaluria type 1. Plos Biol. 10: e1001309.

Gabay-Maskit, S., Cruz-Zaragoza, L.D., Shai, N., Eisenstein, M., Bibi, C., Cohen, N., Hansen, T., Yifrach, E., Harpaz, N., Belostotsky, R., et al. (2020). A piggybacking mechanism enables peroxisomal localization of the glyoxylate cycle enzyme Mdh2 in yeast. J. Cell Sci. 133: 244376.

Gatto, G.J., Geisbrecht, B.V., Gould, S.J., and Berg, J.M. (2000). Peroxisomal targeting signal-1 recognition by the TPR domains of human PEX5. Nat. Struct. Biol. 7: 1091–1095.

Gerondopoulos, A., Bräuer, P., Sobajima, T., Wu, Z., Parker, J.L., Biggin, P.C., Barr, F.A., and Newstead, S. (2021). A signal capture and proofreading mechanism for the KDEL-receptor explains selectivity and dynamic range in ER retrieval. Elife 10, https://doi.org/10.7554/eLife.68380.

Hagen, S., Drepper, F., Fischer, S., Fodor, K., Passon, D., Platta, H.W., Zenn, M., Schliebs, W., Girzalsky, W., Wilmanns, M., et al. (2015). Structural insights into cargo recognition by the yeast PTS1 receptor. J. Biol. Chem. 290: 26610–26626.

Hanscho, M., Ruckerbauer, D.E., Chauhan, N., Hofbauer, H.F., Krahulec, S., Nidetzky, B., Kohlwein, S.D., Zanghellini, J., and Natter, K. (2012). Nutritional requirements of the BY series of Saccharomyces cerevisiae strains for optimum growth. FEMS Yeast Res. 12: 796–808.

Hegde, R.S. and Zavodszky, E. (2019). Recognition and degradation of mislocalized proteins in health and disease. Cold Spring Harbor. Perspect. Biol. 11: a033902.

Hochreiter, B., Chong, C.-S., Hartig, A., Maurer-Stroh, S., Berger, J., Schmid, J.A., and Kunze, M. (2020). A novel FRET approach quantifies the interaction strength of peroxisomal targeting signals and their receptor in living cells. Cells 9: 2381.

Islinger, M., Voelkl, A., Fahimi, H.D., and Schrader, M. (2018). The peroxisome: an update on mysteries 2.0. Histochem. Cell Biol. 150: 443–471.

James, P., Halladay, J., and Craig, E.A. (1996). Genomic libraries and a host strain designed for highly efficient two-hybrid selection in yeast. Genetics 144: 1425–1436.

Janke, C., Magiera, M.M., Rathfelder, N., Taxis, C., Reber, S., Maekawa, H., Moreno-Borchart, A., Doenges, G., Schwob, E., Schiebel, E., et al. (2004). A versatile toolbox for PCR-based tagging of yeast genes: new fluorescent proteins, more markers and promoter substitution cassettes. Yeast 21: 947–962.

Kerssen, D., Hambruch, E., Klaas, W., Platta, H.W., de Kruijff, B., Erdmann, R., Kunau, W.-H., and Schliebs, W. (2006). Membrane association of the cycling peroxisome import receptor Pex5p. J. Biol. Chem. 281: 27003–27015.

Konopka, J.B. (1993). AFR1 acts in conjunction with the alpha-factor receptor to promote morphogenesis and adaptation. Mol. Cell Biol. 13: 6876–6888.

Kunze, M., Kragler, F., Binder, M., Hartig, A., and Gurvitz, A. (2002). Targeting of malate synthase 1 to the peroxisomes of Saccharomyces cerevisiae cells depends on growth on oleic acid medium. Eur. J. Biochem. 269: 915–922.

Lametschwandtner, G., Brocard, C., Fransen, M., Van Veldhoven, P., Berger, J., and Hartig, A. (1998). The difference in recognition of terminal tripeptides as peroxisomal targeting signal 1 between yeast and human is due to different affinities of their receptor Pex5p to the cognate signal and to residues adjacent to it. J. Biol. Chem. 273: 33635–33643.

Laurila, K. and Vihinen, M. (2009). Prediction of disease-related mutations affecting protein localization. BMC Genom. 10: 122.

Pettersen, E.F., Goddard, T.D., Huang, C.C., Couch, G.S., Greenblatt, D.M., Meng, E.C., and Ferrin, T.E. (2004). UCSF Chimera—a visualization system for exploratory research and analysis. J. Comput. Chem. 25: 1605–1612.

Rosenthal, M., Metzl-Raz, E., Bürgi, J., Yifrach, E., Drwesh, L., Fadel, A., Peleg, Y., Rapaport, D., Wilmanns, M., Barkai, N., et al. (2020). Uncovering targeting priority to yeast peroxisomes using an in-cell competition assay. Proc. Natl. Acad. Sci. U.S.A. 117: 201920078.

Šali, A. and Blundell, T.L. (1993). Comparative protein modelling by satisfaction of spatial restraints. J. Mol. Biol. 234: 779–815.

Schaeffer, C., Creatore, A., and Rampoldi, L. (2014). Protein trafficking defects in inherited kidney diseases. Nephrol. Dial. Transplant. 29: iv33–iv44.

Schreiber, G. and Keating, A.E. (2011). Protein binding specificity versus promiscuity. Curr. Opin. Struct. Biol. 21: 50–61.

Stanley, W.A., Filipp, F.V., Kursula, P., Schüller, N., Erdmann, R., Schliebs, W., Sattler, M., and Wilmanns, M. (2006). Recognition of a functional peroxisome type 1 target by the dynamic import receptor Pex5p. Mol. Cell 24: 653–663.

Tong, A.H. and Boone, C. (2006). Synthetic genetic array analysis in *Saccharomyces cerevisiae*. Methods Mol. Biol. 313: 171–192.

Trinquier, G. and Sanejouand, Y.H. (1998). Which effective property of amino acids is best preserved by the genetic code? Protein Eng. 11: 153–169.

Van Der Spoel, D., Lindahl, E., Hess, B., Groenhof, G., Mark, A.E., and Berendsen, H.J.C. (2005). GROMACS: fast, flexible, and free. J. Comput. Chem. 26: 1701–1718.

Walter, T. and Erdmann, R. (2019). Current advances in protein import into peroxisomes. Protein J. 38: 351–362.

Weill, U., Yofe, I., Sass, E., Stynen, B., Davidi, D., Natarajan, J., Ben-Menachem, R., Avihou, Z., Goldman, O., Harpaz, N., et al. (2018). Genome-wide SWAp-Tag yeast libraries for proteome exploration. Nat. Methods 15: 617–622.

Yifrach, E., Chuartzman, S.G., Dahan, N., Maskit, S., Zada, L., Weill, U., Yofe, I., Olender, T., Schuldiner, M., and Zalckvar, E. (2016). Characterization of proteome dynamics during growth in oleate reveals a new peroxisome-targeting receptor. J. Cell Sci. 129: 4067–4075.

Yifrach, E., Holbrook-Smith, D., Bürgi, J., Othman, A., Eisenstein, M., Van Roermund, C.W.T., Visser, W., Tirosh, A., Bibi, C., Galor, S., et al. (2021). Systematic multi-level analysis of an organelle proteome reveals new peroxisomal functions. bioRxiv, Rehovot.

Yofe, I. and Schuldiner, M. (2014). Primers-4-Yeast: a comprehensive web tool for planning primers for Saccharomyces cerevisiae. Yeast 31: 77–80.

Yofe, I., Weill, U., Meurer, M., Chuartzman, S., Zalckvar, E., Goldman, O., Ben-Dor, S., Schutze, C., Wiedemann, N., Knop, M., et al. (2016). One library to make them all: streamlining the creation of yeast libraries via a SWAp-Tag strategy. Nat. Methods 13: 371–378.

Supplementary Material: The online version of this article offers supplementary material (https://doi.org/10.1515/hsz-2022-0116).